

Learning Human Kinematics by Modeling Temporal Correlations between Joints for Video-based Human Pose Estimation

Yonghao Dang, Jianqin Yin *Member, IEEE*, Shaojie Zhang, Jiping Liu, and Yanzhu Hu

Abstract—Estimating human poses from videos is critical in human-computer interaction. By precisely estimating human poses, the robot can provide an appropriate response to the human. Most existing approaches use the optical flow, RNNs, or CNNs to extract temporal features from videos. Despite the positive results of these attempts, most of them only straightforwardly integrate features along the temporal dimension, ignoring temporal correlations between joints. In contrast to previous methods, we propose a plug-and-play kinematics modeling module (KMM) based on the domain-cross attention mechanism to model the temporal correlation between joints across different frames explicitly. Specifically, the proposed KMM models the temporal correlation between any two joints by calculating their temporal similarity. In this way, KMM can learn the motion cues of each joint. Using the motion cues (temporal domain) and historical positions of joints (spatial domain), KMM can infer the initial positions of joints in the current frame in advance. In addition, we present a kinematics modeling network (KIMNet) based on the KMM for obtaining the final positions of joints by combining pose features and initial positions of joints. By explicitly modeling temporal correlations between joints, KIMNet can infer the occluded joints at present according to all joints at the previous moment. Furthermore, the KMM is achieved through an attention mechanism, which allows it to maintain the high resolution of features. Therefore, it can transfer rich historical pose information to the current frame, which provides effective pose information for locating occluded joints. Our approach achieves state-of-the-art results on two standard video-based pose estimation benchmarks. Moreover, the proposed KIMNet shows some robustness to the occlusion, demonstrating the effectiveness of the proposed method.

Index Terms—Human pose estimation, relational modeling, key-point detection, deep learning.

I. INTRODUCTION

HUMAN pose estimation (HPE) is a fundamental component in artificial intelligence systems. Detecting human poses, for example, is critical for intelligent robots to adjust their actions and allocate their attention properly when interacting with humans [1]. Moreover, HPE has been widely

exploited for many computer vision tasks, such as action recognition [2], [3], virtual reality [4], and human-computer interaction [5]–[7]. According to the data source type, HPE can be roughly divided into two scopes, i.e., image-based HPE and video-based HPE. Unlike images, videos not only contain the appearance features for each frame but also encompass rich temporal information. Therefore, for estimating poses from videos, it is significant to model the temporal information effectively.

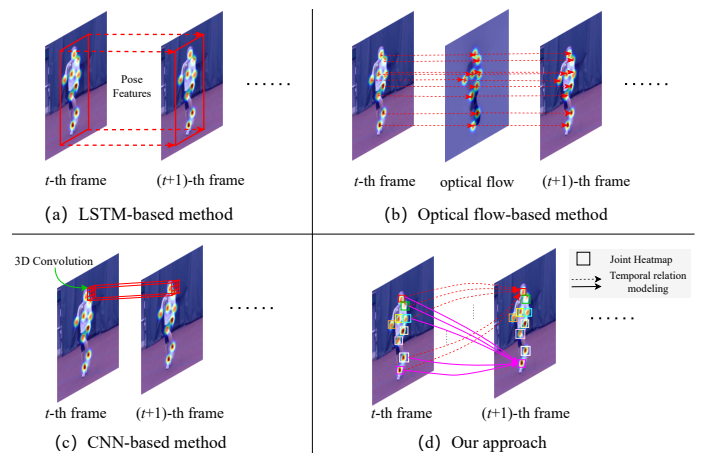


Fig. 1. Comparisons between our approach and other existing methods. (a) LSTM-based methods tend to integrate the high-level pose features along the temporal dimension. (b) Optical flow-based approaches usually use flow information to align joints in different frames. (c) CNN-based methods aggregate features over a convolutional kernel along the temporal dimension. (d) Different from existing methods, our approach can model the temporal correlation between any two joints across different frames.

Due to its remarkable progress in the computer vision community, deep learning has been commonly used to model temporal information for video-based HPE. Long short-term memory (LSTM) [8], optical flow [9]–[11], and convolutional neural networks (CNNs) [12]–[15] have been generally applied to extract temporal features from videos. Despite the positive results shown in previous methods, there is a common important yet neglected factor among these approaches. Lots of existing approaches have the limited ability to model temporal correlations between joints explicitly.

As shown in Fig. 1, LSTM-based methods aggregate vanilla sequential features of poses in adjacent frames [1]. Optical flow-based approaches leverage the flow-based motion information to align the joints in different frames. 3D CNN-

Corresponding author: Jianqin Yin

Yonghao Dang, Jianqin Yin, and Shaojie Zhang are with the School of Artificial Intelligence, Beijing University of Posts and Telecommunications, Beijing 100876, China (e-mail: dyh2018@bupt.edu.cn; jqyin@bupt.edu.cn; zsj@bupt.edu.cn).

Jiping Liu is with the Chinese Academy of Surveying and Mapping, Beijing 100830, China, Faculty of Geosciences and Environmental Engineering, Southwest Jiaotong University, Chengdu 610031, China, and School of Resource and Environmental Sciences, Wuhan University, Wuhan 430079, China.

Yanzhu Hu is with the School of Modern Post (School of Automation), Beijing University of Posts and Telecommunications, Beijing 100876, China.

based methods integrate features over a convolutional kernel along the temporal dimension. Besides, in order to model the temporal semantic consistency of videos, [14], [15] utilize 2D convolutional modules to obtain the high-level representation of the previous frame and transmit it to the next frame. However, the reduction of feature maps' resolution can cause the loss of spatial information to some extent during transferring pose features.

Furthermore, methods mentioned above are mainly constrained to simply sequential relations based on pose features, which ignores the explicit modeling of temporal correlations between different joints. The temporal correlations between joints are significant for locating joints. Especially for the occluded joints, if the temporal correlation of joints can be captured, the model can infer the positions of occluded joints according to the correlation between them at present and those visible joints at the previous moment. Therefore, it is necessary to consider temporal correlations between joints during estimating human poses from videos.

In this paper, we propose a **KN**ematics **M**odeling based **N**etwork (KIMNet) to tackle the above challenges. Different from previous methods, the proposed KIMNet explicitly models the temporal correlation between any two joints across different frames, as shown in Fig. 1 (d). In this way, the KIMNet can learn the features of human kinematics, i.e., the motion cue of each joint relative to all joints in the previous frame. To achieve above objectives, the proposed KIMNet adopts a frame-by-frame processing framework, as shown in Fig.2. Moreover, we present a novel and plug-and-play kinematic modeling module (KMM) based on the domain-cross attention mechanism to model temporal correlations between joints explicitly. The KMM takes pose features in two adjacent frames and joints' heatmaps in the previous frame as inputs and then computes the temporal similarity of pose features to model temporal correlations between joints. By integrating temporal correlations and positions of joints, KMM can infer the initial positions of joints from the current frame, even if joints are occluded. Finally, KIMNet uses the pose features of the current frame to balance the uncertainty contained by initial positions for locating current joints. Unlike traditional self-attention mechanisms that receive features from the same field, the KMM can effectively fuse features from different domains, such as the temporal correlation between joints from the temporal domain and joints' heatmaps from the spatial domain (details are described in Section III). Furthermore, the KMM maintains the high resolution of pose features during modeling the temporal information, avoiding the loss of spatial information caused by the decline of the resolution. Thanks to the above advantages, our KIMNet shows robustness to the occlusion.

Contributions of this work are summarized as follows.

- We propose a plug-and-play kinematics modeling module (KMM) based on the domain-cross attention mechanism to explicitly model the temporal correlation between joints across different frames. The KMM can infer the

initial positions of joints by fusing the temporal correlation of joints (temporal domain) and joints' heatmaps (spatial domain). Furthermore, KMM maintains the high resolution of pose features of historical frames allowing it to transfer rich pose information to future frames.

- We present a **KN**ematics **M**odeling based **N**etwork (KIMNet) to learn the human kinematic characteristics by explicitly modeling the temporal correlation between joints. Benefit from the temporal correlation between joints, KIMNet can locate the occluded joints at the current time according to the joints at the historical time.
- The proposed KIMNet achieves the new state-of-the-art performance among methods on the challenging Penn Action and Sub-JHMDB datasets. Furthermore, the KMM is compatible with existing pose estimation frameworks, which demonstrates the effectiveness of the proposed approach.

II. RELATED WORK

A. Video-based Human Pose Estimation

Human pose estimation has always been one of the hot issues in computer vision tasks. With the improvement of deep learning, image-based pose estimation [16]–[22] has made great progress. However, image-based methods are difficult to be directly applied to video-based pose estimation due to the lack of temporal modeling. Therefore, there has been a lot of research for video-based human pose estimation in recent years.

a) Hand-craft feature based methods: Inspired by the sequential modeling in natural language processing, Park et al. [23] designed a quad representation for each body part and extended the previous N-best algorithm from the speech community to incorporate non-maximal suppression cues. Nie et al. [24] designed a spatial-temporal And-Or graph model based on three types of manual features and used a support vector machine (SVM) to solve the problem of pose estimation in videos. These methods heavily depend on the hand-craft features, which increases the labor cost and is easily limited in the human subjective factors.

b) Optical flow-based methods: Pfister et al. [10] proposed to use optical flow to model the temporal features of poses in videos. They used fully convolutional network to extract spatial features of each frame and optical flow to align joints in continuous frames. Charles et al. [25] utilized graph matching based on the optical flow to connect joints from different frames, which lays the foundation for the graph matching-based human pose estimation. Song et al. [26] presented to compute the dense optical flow between frames and used a flow-based warping layer to align joints. Hwang et al. [27] introduced temporal flow maps for limbs to track human poses from videos. Although these methods have achieved attractive results, the optical flow calculation needs a high computational cost.

c) LSTM-based methods: Recurrent neural networks have shown superior sequential modeling performance, but the ability to extract spatial features is limited. Therefore, some works have combined the RNN and CNN to model spatial-temporal features of poses. Luo et al. [8] built a multi-stage

ConvLSTM that combines the CPM [16] and LSTM [28] to capture the spatial features and temporal geometric consistency among video frames for pose estimation. Similarly, Li et al. [29] rewrote the weight-sharing CNN as a recurrent network to estimate poses from continuous images. Okada et al. [30] designed a recurrent architecture to utilize time-sequence information of poses to manage difficult situations, such as the frequent disappearance and reappearances of poses. Artacho et al. [31] proposed UniPose-LSTM adopting a linear sequential LSTM configuration with the waterfall-based approach for temporal human pose estimation in videos. LSTM suffers from the dilemma of error accumulation. Furthermore, LSTM-based methods are mainly constrained to simply sequential correlation based on pose features.

d) CNN-based methods: Xiao et al. [32] provided a simple baseline based on the ResNet for human pose estimation. Girdhar et al. [33] and Wang et al. [34] used 3D Mask R-CNN and 3D HRNet to model the spatial-temporal features of poses. Jin et al. [35] presented a unified framework consisting of a SpatialNet and a TemporalNet for multi-person pose estimation and tracking. To improve the model's efficiency, Nie et al. [14] formulated pose estimation in videos as the feature matching. They proposed a dynamic kernel distillation (DKD) to capture the temporal dependency of poses. Zhang et al. [36] pointed out that videos have a lot of redundant information. Thus, they proposed a key frame proposal network (KPN) to remove the redundant frames of videos and extract distinguishing spatial-temporal representations of poses.

B. Relation Modeling in Pose Estimation

Most studies about relation modeling in pose estimation pay attention to the spatial relations of poses within a single frame. Bulat et al. [37] used two stages CNN-based framework to detect body parts. To process the occlusion in videos, Fu et al. [38] applied a graphical occlusion model to encode self-occlusion and occlusion by other objects by modeling the interaction between body parts and objects. Ning et al. [39] presented a fractal network for human pose estimation to capture the multiscale interdependence between joints. Wang et al. [40] utilized a graphical neural network to model the physical connection between joints. Bin et al. [41] built a directed graph between body keypoints represented by a 3D tensor according to the natural connection of joints. Most of these methods heavily depend on manual graphs to model the relationship between joints, preventing the model from learning sufficient pose structural information. Dang et al. [15] designed a lightweight joint relation module to automatically and explicitly model the correlation between any two joints. The above methods only focus on the spatial association between joints.

To sum up, there is still a challenge in the existing approaches for human pose estimation in videos. Most methods ignore the explicit modeling of the temporal correlation between different joints, which is meaningful for video-based human pose estimation. Different from previous methods, our proposed KIMNet can explicitly model the temporal correlation between

any two joints across different frames, effectively improving the performance of the model.

III. METHODOLOGY

In this section, we introduce KIMNet, a model dedicated to estimating poses from videos, which leverages human kinematic characteristics to model pose motion cues. To achieve this goal, we present a kinematic modeling module that is specially used to capture the motion cues of poses by explicitly modeling the temporal correlations between joints in different frames.

A. Problem Statement

Given the input sequence that consists of a series of sequential frames randomly sampled from the video, i.e., $\mathcal{I} = \{I_t, I_{t+1}, \dots, I_{t+T}\}$, where $I_t \in \mathbb{R}^{H \times W \times 3}$. t represents the t -th frame. T is the number of input frames. H and W are the height and width of the input frame. The KIMNet aims at generating heatmaps of joints, i.e., $\mathcal{M} = \{M_t, M_{t+1}, M_{t+T}\}$, from all frames, where $M_t = \{m_t^1, m_t^2, \dots, m_t^K\}$. K is the number of joints. The final positions of joints ($\mathcal{J} = \{J_t, J_{t+1}, \dots, J_{t+T}\}$, where $J_t = \{j_t^1, j_t^2, \dots, j_t^K\}$) can be obtained by taking the maximum of \mathcal{M} .

Because actions are continuous in videos, positions of joints at present are related to those at the last time. If the offset $\mathcal{O}_{t,t+1}$ between joints across different frames is learned, positions of joints in the $(t+1)$ -th frame \mathcal{P}_{t+1} can be inferred by combining with the positions of joints in the t -th frame \mathcal{P}_t . However, there are some uncertainties in the inferred joints due to the lack of the information about the $(t+1)$ -th frame. Therefore, it is necessary to balance these uncertainties with the information of the $(t+1)$ -th frame. Formally,

$$\mathcal{P}_{t+1} = \psi(\mathcal{O}_{t,t+1}, \mathcal{P}_t) + \mathcal{F}_{t+1} \quad (1)$$

where $\psi(\cdot)$ represents the inference function that is used to infer the positions of joints in the $(t+1)$ -th frame. \mathcal{F}_{t+1} is the information contained by the $(t+1)$ -th frame. In practice, we apply the convolutional networks to fit Eq. 1.

B. Overview of KIMNet

Inspired by [15], we design a kinematics modeling based network that consists of three main stages, as summarized in Fig. 2. Although the overall structure is similar to [15], there is obvious difference between tow approaches. [15] models the spatial correlations between joints in the same frame, while the proposed KIMNet aims at modeling the temporal correlations between joints across different frames. Next, we introduce the KIMNet in detail.

a) Encoding human poses: As we described in subsection A, KIMNet utilizes historical positions of joints and pose features in the current frame to locate joints in the current frame. Therefore, we use a pretrained pose initializer to get initial positions of joints (m_1^p) from the first frame and a feature encoder to extract pose features (f_t) from all frames.

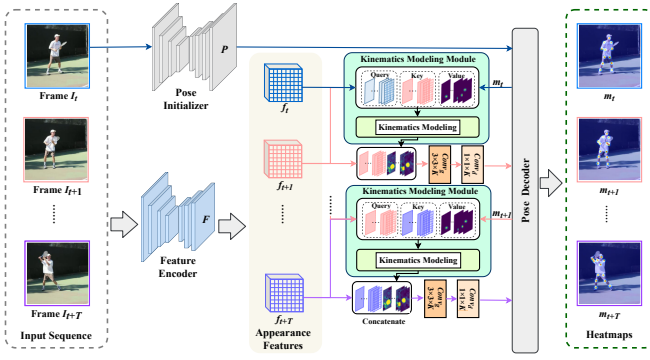


Fig. 2. Overview of the proposed kinematics modeling network. For the 1st frame, the pose initializer P and feature encoder F are used to generate the initial heatmaps of joints and extract appearance features of poses. Then, the pose decoder (e.g. the JRE [15]) is applied to produce the final heatmaps for joints. For subsequent frames, KMM takes pose features f_t , f_{t+1} , and heatmaps of joints m_t in the t -th frame as inputs to infer the initial positions of joints in the current frame m_{t+1}^p . Next, f_{t+1} is used to eliminate uncertainties contained by m_{t+1}^p . Finally, the pose decoder is applied to generate the final pose.

b) Kinematics modeling: Human motion cues are significant for estimating poses in videos. If the motion cues can be modeled effectively, it is possible to infer positions of joints from the $(t+1)$ -th frame with the help of positions of joints in the t -th frame before obtaining the final joints. Based on this conjecture, we propose a kinematic modeling module (KMM) based on the domain-cross attention mechanism to explore motion cues of each joint by modeling the temporal correlation between joints. Then the motion cues of each joint are integrated with its historical position to infer positions from the current frame.

Motion cues modeling aims to capture the motion information for each joint. Pose representations f_t in different frames can be obtained by the feature encoder as we mentioned above. Based on f_t that contains the information about each joint, we can capture the motion information of each joint by modeling the correlation between any two joints. In practice, joints are represented by a set of heatmaps consisting of $h \times w$ pixels. Therefore, the motion of the whole heatmap, that is, the motion of all pixels, should be modeled to represent the motion of the joint. Considering that the dot-product is essentially a weighted sum, it can integrate the information of all pixels in the heatmap. Thus, it can reflect the motion of the whole heatmap to some extent. And the dot-product can measure the correlation [42]. Therefore, we use dot-product to model the temporal correlation between any two joints.

$$O_{t,t+1} = \text{Sim}(f_t, f_{t+1}), t = 1, 2, \dots, T-1 \quad (2)$$

where $O_{t,t+1} \in \mathbb{R}^{K \times K}$ represents the change of poses in I_{t+1} relative to the poses in I_t . $\text{Sim}(\cdot)$ is the similarity calculation based on the dot-product. The softmax operation then is used to turn the temporal correlation $O_{t,t+1}$ to the temporally correlational attention for the convenient combination with the historical positions of joints. Details can be found in subsection C.

$O_{t,t+1}$ contains the motion information about each joint, and m_t includes the positional information of joints in the t -th frame. According to the positional information and motion cues of joints, the model can preliminarily infer the positions of joints from the $(t+1)$ -th frame.

$$m_{t+1}^p = \psi(O_{t,t+1}, m_t), t = 1, 2, \dots, T-1 \quad (3)$$

where $m_{t+1}^p \in \mathbb{R}^{h \times w \times K}$ is the initial heatmaps of joints. $\psi(\cdot)$ is the inference function. Because $O_{t,t+1}$ contains the temporally correlational attention between the joint J_{t+1}^j and all joints in the t -th frame, the initial position of J_{t+1}^j can be obtained through the weighted sum of $O_{t,t+1}$ and m_t . Therefore, we also take the dot-product as the inference function $\psi(\cdot)$.

c) Estimating keypoints: To obtain the precise heatmaps for joints, we apply a pose decoder to produce the final heatmaps. For the first frame, the pose decoder is directly applied to m_1^p predicted by the pose initializer to get the final pose.

For subsequent frames, there are some uncertainties in predicted heatmaps m_{t+1}^p due to the lack of pose information of the $(t+1)$ -th frame. Therefore, we use f_{t+1} to alleviate these uncertainties. Practically, we adopt two stacked convolutional layers including a 3×3 and a 1×1 convolutions that are described as Conv_g and Conv_d to introduce f_{t+1} into m_{t+1}^p . After Conv_g and Conv_d , we can get the coarse- and fine-grained pose features, respectively.

$$\begin{aligned} f_{t+1}^{\text{coarse}} &= \sum_{i=1}^K w_{\text{conv}_g}^i * m_{t+1}^p + \sum_{j=K+1}^D w_{\text{conv}_g}^j * f_{t+1} \\ f_{t+1}^{\text{fine}} &= \sum_{i=1}^K w_{\text{conv}_d}^i * f_{t+1}^{\text{coarse}} \end{aligned} \quad (4)$$

where $f_{t+1}^{\text{coarse}} \in \mathbb{R}^{h \times w \times D}$ and $f_{t+1}^{\text{fine}} \in \mathbb{R}^{h \times w \times K}$ represent the coarse- and fine-grained pose representations, respectively. $w_{\text{conv}_g}^i \in \mathbb{R}^{3 \times 3}$ and $w_{\text{conv}_d}^i \in \mathbb{R}^{1 \times 1}$ are convolutional filters in Conv_g and Conv_d . And $*$ represents the convolutional operation.

Finally, the pose decoder is used to produce the final heatmap for each joint.

$$m_{t+1} = \text{Decoder}(f_{t+1}^{\text{fine}}), t = 1, 2, \dots, T-1 \quad (5)$$

C. Kinematics Modeling Module

In order to model the temporal correlation between joints, we present a plug-and-play kinematics modeling module (KMM) based on the domain-cross attention mechanism, as shown in Fig. 3. Different from traditional self-attention, the proposed KMM can make a fusion of the temporal correlation between joints from the temporal domain and heatmaps of joints from the spatial domain. Next, details of the KMM will be described.

a) Robust pose representations extraction: KMM takes pose features f_t , f_{t+1} and joints' heatmap m_t as inputs. There is a certain spatial similarity for two adjacent frames, i.e., the appearance of the person keeps unchanged, and the pose only changes slightly. Therefore, features f_t is analogous to

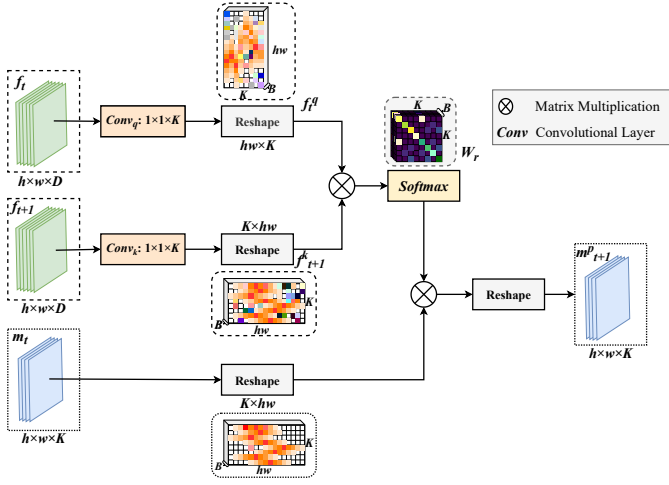


Fig. 3. The structure of the proposed kinematics modeling module. Two 1×1 convolutions ($Conv_q$ and $Conv_k$) are used to extract discriminative pose features. Matrix multiplication is applied to the reshaped f_t^q and f_{t+1}^k to calculate the temporal correlation between any two joints. Then the softmax normalizes the temporal correlation to the attention map that contains the motion cues of poses between contiguous frames. By combining the motion cues and the historical positions of joints m_t , KMM can infer the initial positions of joints in the $(t+1)$ -th frame, i.e., m_{t+1}^p .

f_{t+1} to some extent. To capture conspicuous motion cues of poses, we adopt two independent 1×1 convolutions marked as $Conv_q$ and $Conv_k$ to extract discriminative pose features from f_t and f_{t+1} . Then reshaping operation is used to convert the feature matrixes into feature vectors for facilitating the temporal correlation modeling.

$$\begin{aligned}
 f_t &= [f_t^1, f_t^2, \dots, f_t^D] \in \mathbb{R}^{h \times w \times D} \\
 f_{t+1} &= [f_{t+1}^1, f_{t+1}^2, \dots, f_{t+1}^D] \in \mathbb{R}^{h \times w \times D} \\
 W_Q &= [w_q^1, w_q^2, \dots, w_q^K] \in \mathbb{R}^{1 \times 1 \times K} \\
 W_K &= [w_k^1, w_k^2, \dots, w_k^K] \in \mathbb{R}^{1 \times 1 \times K} \\
 f_t^q &= \text{Reshape}(\sigma(W_Q * f_t)) \in \mathbb{R}^{(h \times w) \times K} \\
 f_{t+1}^k &= \text{Reshape}(\sigma(W_K * f_{t+1})) \in \mathbb{R}^{K \times (h \times w)}
 \end{aligned} \quad (6)$$

where W_Q and W_K are weights of $Conv_q$ and $Conv_k$. $\sigma(\cdot)$ and $*$ represents the nonlinear function and convolutional operation, respectively. f_t^q and f_{t+1}^k serve as the query set and the key set. As features f_t and f_{t+1} includes the features about the entire pose, f_t^q and f_{t+1}^k contain the information about each joint. And each column in f_t^q and each row f_{t+1}^k can represent one joint.

b) Temporal correlation modeling: Considering that joints are relevant to each other when the person is moving. We model the temporal correlation between any two joints by calculating the similarity between features f_t^q and f_{t+1}^k . The dot-product can measure the similarity between two vectors to some extent [42]. Hence, we apply the dot-product of joints' features to model the temporal correlation between them. For the i -th and j -th joints represented by $f_t^{q_i} \in \mathbb{R}^{(h \times w) \times 1}$ and $f_{t+1}^{k_j} \in \mathbb{R}^{1 \times (h \times w)}$, the temporal correlation between them can be modelled as follows.

$$O_{t,t+1}^{i,j} = f_{t+1}^{k_j} \cdot f_t^{q_i}, t = 1, 2, \dots, T-1 \quad (7)$$

where $O_{t,t+1}^{i,j}$ represents the similarity of the i -th joint in the t -th frame and the j -th joint in the $(t+1)$ -th frame. The dot-

product is essentially a weighted sum of joint heatmaps that reflects the overall motion clue of the joint J_{t+1}^j relative to J_t^i . We can model the temporal correlation between any two joints at different times as Eq.7. This process can be realized by the matrix multiplication as follows.

$$O_{t,t+1} = \left(\frac{f_{t+1}^k \otimes f_t^q}{\sqrt{d}} \right) \in \mathbb{R}^{K \times K}, t = 1, 2, \dots, T-1 \quad (8)$$

where $O_{t,t+1} = \{o_{t,t+1}^{1,1}, o_{t,t+1}^{1,2}, \dots, o_{t,t+1}^{i,j}, \dots, o_{t,t+1}^{K,K}\} \in \mathbb{R}^{K \times K}$ represents the temporal correlations of joints in two different frames. Each element in $O_{t,t+1}$ is the temporal relation between any two joints. d is the normalized factor that is equal to the dimension of features f_t^q and f_{t+1}^k .

In order to enhance the motion cues of the joint J_{t+1}^j relative to the entire pose, the softmax operation, then, is used to model the global correlation [43] that can be regarded as the correlation between the J_{t+1}^j and all joints in the t -th frame.

$$w_r^{l,j} = \frac{1}{\sum_{i=1}^K o_{t,t+1}^{i,j}} \cdot o_{t,t+1}^{l,j}, t = 1, 2, \dots, T-1 \quad (9)$$

where $w_r^{l,j}$ is the temporally correlational weight between J_{t+1}^j and J_t^l . $W_r = \{w_r^{1,1}, w_r^{1,2}, \dots, w_r^{K,K}\} \in \mathbb{R}^{K \times K}$ can pay much attention to the joints that have the high temporal correlation, otherwise, it will provide the low attention weight to joint pairs. Because $o_{t,t+1}^{l,j}$ includes the temporal correlation between two joints across different frames, the sum of $o_{t,t+1}^{i,j}$ integrates temporal correlations of all joint pairs. Therefore, the Eq.9 can reflect the motion information of J_{t+1}^j relative to all joints in the t -th frame to some extent.

c) Inference of joints' initial positions: The motion information of each joint can be learned through the temporal correlation modeling. Based on the known positional information of joints in the t -th frame (M_t), intuitively, positions of J_{t+1} (M_{t+1}^p) can be inferred through the motion information. In practice, we transfer the heatmap M_t to $M_t^v \in \mathbb{R}^{K \times (h \times w)}$ for the convenient inference of M_{t+1}^p . Since W_r includes the motion information of joints, applying W_r to the position of joints in t -th frame can preliminarily infer the k -th joint's position in the next time. The KMM computes the response at a position of J_{t+1}^k as a weighted sum of the positions of all joints, which can be denoted as:

$$\begin{aligned}
 M_t^v &= \{m_t^{v1}, m_t^{v2}, \dots, m_t^{vD}\} \in \mathbb{R}^{K \times (h \times w)} \\
 \bar{M}_{t+1}^p &= W_r \cdot M_t^v \in \mathbb{R}^{K \times (h \times w)}
 \end{aligned} \quad (10)$$

where \bar{M}_{t+1}^p is the initial heatmap vector of joints. The reshaping operation is used to convert \bar{M}_{t+1}^p to the initial heatmap M_{t+1}^p with the shape of $K \times h \times w$.

D. Training Loss Function

In this paper, we minimize the L_2 norm between the output of the model and the heatmap of ground truth to optimize the proposed KIMNet. Specifically,

$$Loss = \frac{1}{N} \sum_{t=1}^N \|M_t - M_t'\|_2^2, t = 1, 2, \dots, N \quad (11)$$

where $M_t = \{m_t^1, m_t^2, \dots, m_t^K\}$ denotes the output of KIMNet. $M'_t = \{m'_t^1, m'_t^2, \dots, m'_t^K\}$ is the joints' heatmap generated according to the ground truth. N is the total number of training frames. $\|\cdot\|$ represents the L_2 norm.

IV. EXPERIMENTS

We first introduce specific experimental settings including datasets, implementation details, and the evaluation metrics. Then, we compare the proposed KIMNet against existing state-of-the-art video-based methods. We also provide ablation studies to confirm the effectiveness of the proposed KMM. Next, we conduct comprehensive experiments about the occlusion to show advantages of the proposed model. Finally, we compare KIMNet with existing state-of-the-art method in non occlusion scenes.

A. Experimental Settings

1) *Datasets*: We evaluate the proposed KIMNet on two challenging video-based datasets including the Penn Action [44] and Sub-JHMDB [45] datasets to demonstrate the effectiveness of the proposed model.

Penn Action dataset contains 2326 video clips. Each frame provides annotations for 13 body joints including head, shoulders, elbows, wrists, hips, knees, and ankles. Besides, Penn Action dataset annotates the position of the person, i.e., the bounding box for each person, and gives the visibility for each joint. Keeping the consistency with [8], [14], [15], we train the model with 1258 video clips, and the others are used to evaluate the model.

Sub-JHMDB dataset includes 316 videos. There are 15 body joints in each frame. Different from the Penn Action dataset, Sub-JHMDB dataset provides the mask for each person instead of the bounding box. Moreover, Sub-JHMDB dataset does not annotate the visibility for each joint. In other words, all joints in the Sub-JHMDB dataset are visible by default. The model is required to locate the occluded joints, which makes it challenging to estimate poses on the Sub-JHMDB dataset. Following [8], [14], [15], 3 fold cross validation is used to evaluate the model. According to existing methods, training sets include 227, 236, and 224 video clips respectively, and testing sets correspondingly contain 89, 80, and 92 samples. To make a fair comparison with previous approaches, we take the average result on three testing sets as the final result.

2) *Implementation details*: Following previous works [14], [15], we take the SimpleBaseline [32] pretrained on the MPII [46] dataset as the pose initializer (ResNet-101) and feature encoder (ResNet-50). Furthermore, to make a fair comparison with existing methods, keeping consistency with works [8], [14], [15], we also: randomly select contiguous 5 frames from each training video clip; adopt the same data augmentation settings as [8], [14], [15] including random scaling, rotation, and flipping; use the Adam [47] optimizer to train the model and the training epoch is set to 100 following [15]. The learning rate is initialized to 0.005, and the batch size is set to 16 on the Penn Action dataset. Because the scale of Sub-JHMDB dataset is smaller than that of Penn Action dataset, the

learning rate and batch size are set to 0.001 and 8, respectively. All experiments are conducted on two NVIDIA GeForce GTX 3080 GPUs.

3) *Evaluation metric*: The percentage of correct keypoints (PCK) is used as the evaluation metric. The PCK for each joint is calculated as follows.

$$PCK_k = \frac{\sum_{n=1}^S \sum_{t=1}^T \eta\left(\frac{d_t^k}{L_t} \leq \alpha\right)}{\sum_{n=1}^S \sum_{t=1}^T 1} \quad (12)$$

where PCK_k is the k -th joint's PCK. S denotes the number of sequences; T is the number of frames in each sequence. $\eta(\cdot)$ is the indicator function. When the condition in parentheses is true, $\eta(\cdot)$ is 1, otherwise it is 0. d_t^k represents euclidean distance between the estimated value and the ground truth of the k -th joint. α is the hyperparameter which is set to 0.2 following [8], [14], [15] to control the range of errors. L_t is the threshold of the error distance. According to [14], [15], we adopt two types of L to evaluate the model: 1) PCK normalized by person size: L is set to the size of the person [8], [14], [15], i.e., $L = \max(H_{bbox}, W_{bbox})$, where H_{bbox} and W_{bbox} are the height and width of the bounding box of the person. 2) PCK normalized by torso size: L is set as the size of the torso that is represented by the distance between the left shoulder and the right hip [14], [15]. Since the size of the torso is smaller than that of the person, the second evaluating method allows smaller error range, which can better reflect the performance of the model. Based on the PCK of each joint, we also use the mean PCK (mPCK) to measure the overall performance of the model [8], [14], [15], as follows.

$$mPCK = \frac{\sum_{n=1}^S \sum_{t=1}^T \sum_{k=1}^K \eta\left(\frac{d_t^k}{L_t} \leq \alpha\right)}{\sum_{n=1}^S \sum_{t=1}^T \sum_{k=1}^K 1} \quad (13)$$

B. Comparison with State-of-the-arts

1) Results on the Penn Action dataset:

a) *PCK normalized by person size*: The proposed KIMNet achieves the best performance on the PCK for each joint and mPCK as shown in TABLE I. The KIMNet outperforms the LSTM [8], K-FPN [36], TCE [49], and DKD [14] by 2.0%, 1.7%, 1.7%, and 1.9% mPCK, respectively. These methods just aggregate features along the temporal dimension but ignore to explicitly model the temporal correlation between joints. In contrast to these methods, the proposed KIMNet models the temporal information of poses by explicitly modeling the temporal correlation between joints, which is beneficial for locating joints. Furthermore, KIMNet achieves better performance than RPSTN including the PCK for each joint and the mPCK for the whole pose. On the one hand, the KIMNet considers the temporal correlation between joints across different frames, while the RPSTN only searches similar regions between two frames. On the other hand, the KMM keeps the high resolution of feature maps which can avoid the loss of spatial information caused by the reduction of the resolution.

TABLE I

COMPARISONS WITH THE STATE-OF-THE-ART METHODS ON THE PENN ACTION DATASET. VALUES IN BRACKETS INDICATE THE GAP BETWEEN THE CORRESPONDING APPROACH AND THE PROPOSED KIMNET.

Methods	Params (M)	Time (ms)	Head	Sho.	Elb.	Wri.	Hip	Knee	Ank.	mPCK
Normalized by person size										
N-Best [23]	-	-	62.8	52.0	32.3	23.3	53.3	50.2	43.0	45.3 (↓ 54.4)
ST-Part [24]	-	-	64.2	55.4	33.8	24.4	56.4	54.1	48.0	48.0 (↓ 51.7)
ACPS [2]	-	-	89.1	86.4	73.9	73.0	85.3	79.9	80.3	81.1 (↓ 18.6)
ChainModel [48]	-	-	95.6	93.8	90.4	90.7	91.8	90.8	91.5	91.8 (↓ 7.9)
Thin-slicing. [26]	-	-	98.0	97.3	95.1	94.7	97.1	97.1	96.9	96.5 (↓ 3.2)
K-FPN. [36]	-	-	98.7	98.7	97.0	95.3	98.8	98.7	98.6	98.0 (↓ 1.7)
TCE [49]	-	-	99.3	98.5	97.6	97.2	98.6	98.1	97.4	98.0 (↓ 1.7)
LSTMPM [8]	231.5	25	98.9	98.6	96.6	96.6	98.2	98.2	97.5	97.7 (↓ 2.0)
DKD [14]	219.92	11	98.8	98.7	96.8	97.0	98.2	98.1	97.2	97.8 (↓ 1.9)
RPSTN [15]	222.17	12	99.0	98.7	98.8	98.5	98.8	98.7	98.8	98.7 (↓ 1.0)
KIMNet (Ours)	214.70	10	99.4	99.6	99.1	99.0	99.8	99.5	99.4	99.7
Normalized by torso size										
LSTMPM [8]	231.5	25	96.0	93.6	92.4	91.1	88.3	94.2	93.5	92.6 (↓ 4.3)
DKD [14]	219.92	11	96.6	93.7	92.9	91.2	88.8	94.3	93.7	92.9 (↓ 4.0)
RPSTN [15]	222.17	12	98.2	96.9	95.2	93.2	96.6	95.7	95.0	95.7 (↓ 1.2)
KIMNet (Ours)	214.70	10	98.6	97.7	96.6	95.7	96.9	97.3	96.3	96.9

b) *PCK normalized by torso size*: As shown in TABLE I, our approach also ranks the first among the existing methods with less parameters and inferencing time. And the overall performance of KIMNet is 1.2% higher than that of RPSTN, which demonstrates the effectiveness of the KIMNet. In particular, we obtain encouraging improvements for those more challenging joints, such as wrists and ankles: with a PCK of 95.7% (↑ 1.8%) for wrists and a PCK of 96.3% (↑ 1.5%) for ankles, confirming the advantages of the KIMNet in locating the challenging joints. Experimental results prove that the temporal correlations between joints are beneficial for estimating poses from videos, which further proves the effectiveness of the KIMNet.

2) *Results on the Sub-JHMDB dataset*: We evaluate the KIMNet on the challenging Sub-JHMDB dataset to further confirm its effectiveness, as shown in TABLE II.

a) *PCK normalized by person size*: We observe that previous approaches have achieved impressive results on the Sub-JHMDB dataset. Specifically, the mPCK of the current state-of-the-art RPSTN is 97.4%. But our KIMNet is able to achieve 98.5% mPCK that surpasses RPSTN by 1.1%. RPSTN only considers the spatial correlation between joints but neglects the temporal association. While the proposed KIMNet models the spatial and temporal correlations between joints simultaneously. Compared with TCE and DKD, the performance of the KIMNet is improved by 2.0% and 4.5%, respectively. TCE and DKD adopt a convolutional module to explore the temporal consistency of videos. It is difficult for convolutions to maintain the complete information about poses due to the reduction of the resolution.

b) *PCK normalized by torso size*: Similar to the results on the Penn Action dataset, our KIMNet also achieves the best performance on the Sub-JHMDB dataset. The advantages of our model over RPSTN are more significant, achieving over 2.3% mPCK improvement. Especially, for the joints with high flexibility, such as elbows, wrists, knees, and ankles, our model achieves 5.0%, 5.3%, 2.9%, and 2.4% improvements over the current state-of-the-art RPSTN, respectively. The reason is that KIMNet can explicitly model the temporal correlation

between joints across different frames while maintaining the high resolution of the feature maps. Experimental results show that modeling spatial and temporal correlations between joints simultaneously is meaningful for estimating human pose from videos.

TABLE II

COMPARISONS WITH THE STATE-OF-THE-ART METHODS ON THE SUB-JHMDB DATASET. VALUES IN BRACKETS INDICATE THE GAP BETWEEN THE CORRESPONDING APPROACH AND THE PROPOSED KIMNET.

Methods	Head	Sho.	Elb.	Wri.	Hip	Knee	Ank.	mPCK
Normalized by person size								
N-Best [23]	79.0	60.3	28.7	16.0	74.8	59.2	49.3	52.5 (↓ 46.0)
ST-Part [24]	80.3	63.5	32.5	21.6	76.3	62.7	53.1	55.7 (↓ 42.8)
ACPS [2]	90.3	76.9	59.3	55.0	85.9	76.4	73.0	73.8 (↓ 24.7)
Thin-slicing [26]	97.1	95.7	87.5	81.6	98.0	92.7	89.8	92.1 (↓ 6.4)
K-FPN [36]	95.1	96.4	95.3	91.3	96.3	95.6	92.6	94.7 (↓ 3.8)
TCE [49]	99.3	98.9	96.5	92.5	98.9	97.0	93.7	96.5 (↓ 2.0)
LSTMPM [8]	98.2	96.5	89.6	86.0	98.7	95.6	90.9	93.6 (↓ 4.9)
DKD [14]	98.3	96.6	90.4	87.1	99.1	96.0	92.9	94.0 (↓ 4.5)
RPSTN [15]	98.9	99.1	99.0	97.9	97.8	97.8	97.3	97.4 (↓ 1.1)
KIMNet (Ours)	98.9	99.1	98.7	98.5	98.6	98.3	97.2	98.5
Normalized by torso size								
LSTMPM [8]	92.7	75.6	66.8	64.8	78.0	73.1	73.3	73.6 (↓ 14.5)
DKD [14]	94.4	78.9	69.8	67.6	81.8	79.0	78.8	77.4 (↓ 10.7)
RPSTN [15]	91.0	87.1	82.1	80.5	88.8	85.9	83.8	85.8 (↓ 2.3)
KIMNet (Ours)	90.1	88.8	87.1	85.8	87.9	88.8	86.2	88.1

C. Ablation Studies

In this section we conduct comprehensive ablation studies to validate the effectiveness of the proposed KIMNet on the Penn Action dataset. We first evaluate the effect of the pose initializer and feature encoder. Then we verify the compatibility of KMM. Next, the rationality of the KMM's structure and the effectiveness of proposed KMM are validated.

1) *Effect of pose initializer and feature encoder*: We remove the pose initializer marked as KIMNet-w/o-P to explore the improvement brought by pose initializer. Then, we adopt various models including SimpleBaseline [32] with different structures (ResNet-18, ResNet-34, and ResNet-50), Hourglass [50], and HRNet [20] as pose initializer and feature encoder to evaluate the influence of different backbones. Experimental

results are listed in TABLE III, where KIMNet[†] is our main approach.

Compared with KIMNet (Res50), the performance of KIMNet-w/o-P degraded by 0.6% mPCK. The positional information of joints in historical time is beneficial for inferring positions of joints. Besides, for different feature encoders, the performance of the proposed KIMNet is improved with the enhancement of feature extraction ability of the feature encoder. The performance achieved by different backbones shows that our KIMNet is compatible for different feature encoders.

TABLE III

ABLATION STUDIES ABOUT THE POSE INITIALIZER AND FEATURE ENCODER. EVALUATION METRIC IS THE PCK NORMALIZED BY TORSO SIZE. KIMNet[†] REPRESENTS THE STRUCTURE USED IN THIS PAPER. VALUES IN BRACKETS INDICATE THE GAP BETWEEN THE CORRESPONDING APPROACH AND THE PROPOSED KIMNet[†].

Methods	Head	Sho.	Elb.	Wri.	Hip	Knee	Ank.	mPCK
KIMNet-w/o-P	97.9	97.1	95.7	95.1	96.6	96.9	95.5	96.3 (↓ 0.6)
KIMNet (Res18)	97.2	97.1	95.0	93.9	96.1	96.2	94.8	95.6 (↓ 1.3)
KIMNet (Res34)	97.6	97.3	95.4	93.3	96.2	96.4	95.0	95.8 (↓ 1.1)
KIMNet [†] (Res50)	98.6	97.7	96.6	95.7	96.9	97.3	96.3	96.9
KIMNet (HG)	98.4	97.7	96.8	95.6	97.2	97.6	97.1	97.1 (↑ 0.2)
KIMNet (HRNet)	98.0	97.8	97.2	95.7	97.3	97.5	97.1	97.2 (↑ 0.3)

2) *Compatibility of KMM*: We integrate KMM into various pose estimation frameworks including LSTMPPM [8], DKD [14], and RPSTN [15], to evaluate its generality, as shown in TABLE IV. Specifically, we replace the temporal modeling modules in raw backbones with the KMM. Because different frameworks pay different attention to joints, the performance of some joint points decreases after integrating KMM. However, the overall performance of the network is improved, which proves that the proposed KMM is compatible with the current popular video-based pose estimation frameworks.

TABLE IV

VERIFICATION OF KMM’S GENERALITY ON THE PENN ACTION DATASET. EVALUATION METRIC IS THE PCK NORMALIZED BY TORSO SIZE.

Methods	Head	Sho.	Elb.	Wri.	Hip	Knee	Ank.	mPCK
LSTMPPM [8]	96.0	93.6	92.4	91.1	88.3	94.2	93.5	92.6 (↓ 0.4)
LSTMPPM-KMM	97.3	94.3	92.3	93.9	89.8	94.5	91.3	93.0
DKD [14]	96.6	93.7	92.9	91.2	88.8	94.3	93.7	92.9 (↓ 0.8)
DKD-KMM	97.7	96.4	91.5	96.2	89.7	95.4	91.4	93.7
RPSTN [15]	98.2	96.9	95.2	93.2	96.6	95.7	95.0	95.7 (↓ 0.2)
RPSTN-KMM	97.9	97.0	94.8	93.3	96.6	96.9	95.9	95.9

TABLE V

ABLATION STUDIES ABOUT THE RATIONALITY OF KMM’S DESIGN. EVALUATION METRIC IS THE PCK NORMALIZED BY TORSO SIZE. VALUES IN BRACKETS INDICATE THE GAP BETWEEN THE CORRESPONDING APPROACH AND OUR METHOD.

Method	Head	Sho.	Elb.	Wri.	Hip	Knee	Ank.	mPCK
KIMNet-Share-QK	97.4	97.1	95.0	93.1	96.8	96.7	95.1	95.8 (↓ 1.1)
KIMNet-w/o-d	97.5	97.1	94.9	93.7	96.4	96.4	95.3	95.8 (↓ 1.1)
KIMNet-Residual	97.4	95.7	88.9	81.1	94.8	91.8	85.9	90.3 (↓ 6.6)
KIMNet-Heatmap	96.2	94.9	86.3	82.5	95.6	92.8	87.6	90.4 (↓ 6.5)
KIMNet (Ours)	98.6	97.7	96.6	95.7	96.9	97.3	96.3	96.9

3) *Rationality of KMM’s design*: We have carried out a comprehensive analysis about the structure of KMM. Experimental results are recorded in TABLE V. **Influence of Conv_q and Conv_k**: we adopt two 1 × 1 convolutions whose weights are shared to generate query set and key set, i.e.,

KIMNet-Share-QK in TABLE V. As can be seen that the performance of KIMNet-Share-QK decreases by 1.1% mPCK over that of KIMNet. Two independent convolutions can extract discriminative pose features from two similar contiguous frames, which is beneficial for learning the change of joints. **Influence of the normalized factor d** : KIMNet-w/o-d denotes the KIMNet without the normalized factor. The normalized factor d brings 1.1% improvement for the KIMNet as the normalized features are conducive to training the model. **Influence of historical heatmaps**: we introduce the residual value set (heatmaps in t -th frame) into KMM for evaluating the influence of historical position on inferring the location of joints in the future, i.e., KIMNet-Residual. The performance decreases obviously after introducing the historical position of joints. We think that m_{t+1}^p has included the positional information about joints in the $(t+1)$ -th frame. The model pays much attention to the historical position of joints after introducing historical positions, which covers up the positional information of the $(t+1)$ -th frame. **Temporal correlations between heatmaps**: we adopt heatmaps in two frames to model the temporal correlation between joints, i.e., KIMNet-Heatmap. The performance of KIMNet-Heatmap also decreases a lot. Compared with joints’ heatmaps which include positional information, pose features f contain rich semantic information about joints, including appearance features and positional information, which is helpful for learning the robust temporal correlations.

4) *Effectiveness of KMM*: To demonstrate the effectiveness of the KMM, we compare the proposed KMM with previous temporal modeling modules, as shown in TABLE VI. We adopt the DKD proposed in [14] and JRPSP introduced by [15] to model the temporal information. Compared with KIMNet-DKD and KIMNet-JRPSP, the proposed KMM brings a 1.1% and 0.9% improvement in the overall performance. Especially for flexible wrists and ankles, the improvement is obvious. These joints generally move violently and are easily prone to motion blur. It is helpful to infer the position of these joints by using the temporal correlation between these flexible joints and others.

D. Qualitative Analysis about Features Learned by KMM

1) *Visualization of temporal correlation*: To intuitively show the temporal correlation learned by KMM, we select one joint from each frame (2^{nd} to 5^{th} frame) and visualize their temporal association on the input sequence, as shown in Fig. 4. The 1^{st} , 3^{rd} , and 5^{th} rows display temporal associations of joints that are visualized according to the 2^{nd} , 4^{th} , and 6^{th} rows, the temporally correlational weights. Different lines indicate different temporal correlations. Red lines denote strong temporal correlations. For the temporally correlational weights, the brighter the color, the stronger the temporal correlation. Dark areas indicate weak correlations, but their actual values are not zero. Therefore, we use light-colored lines to represent the weak correlation in the input sequence.

As shown in Fig.4, the KMM can pay similar attention to the same poses. For example, the temporal correlations of joints are similar in the action “play golf.” While there are

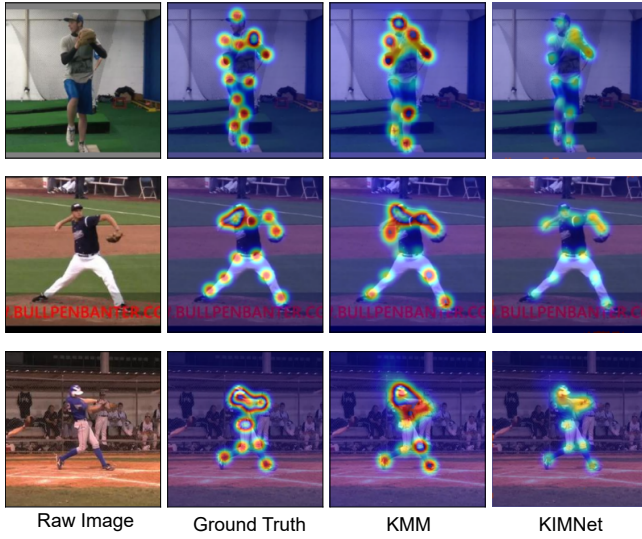


Fig. 6. Outputs of the proposed KMM and KIMNet. The visualization results from left to right are the original input frames, heatmaps of ground truth, outputs of the KMM, and outputs of the KIMNet.



Fig. 7. Visualization of the temporal occlusion.

a) Verification of temporal occlusion: We randomly select a frame from the input sequence and generate two masks to occlude joints. Experimental results of the proposed KIMNet and RPSTN are shown in Fig.7. For the first group of actions (the first three rows in Fig.7), the left shoulder and neck estimated by RPSTN are crowded together due to the occlusion of these joints in the 2^{nd} frame. Moreover, the neck and shoulder in subsequent frames are also inaccurate due to the lack of temporal correlation modeling of joints. On the contrary, because our proposed KIMNet explicitly models the temporal correlation between joints across different frames, it can use all joints in the previous frame to help locate the joint in the current frame. Therefore, KIMNet can locate joints accurately even if they are occluded. For the second group of actions (the

last three rows in Fig.7), the head and shoulders in the last frame are blocked. Similarly, RPSTN locates occluded joints inaccurately. While the KIMNet provides accurate positions for occluded joints with the help of joints in the previous frame.

b) Verification of spatial occlusion: To explore the potential of KIMNet for occlusion, we randomly generate two masks from the 2^{nd} to the T^{th} frame, as shown in Fig.8. Because the spatial information of the occluded pose is missing, it is difficult for RPSTN to match similar regions in adjacent frames. Therefore, RPSTN provides inferior results for occluded joints from the 2^{nd} to the T^{th} frame. However, the proposed KIMNet can utilize all joints in the 1^{st} frame to locate occluded joints. It can provide reasonable positions for occluded joints in subsequent frames.

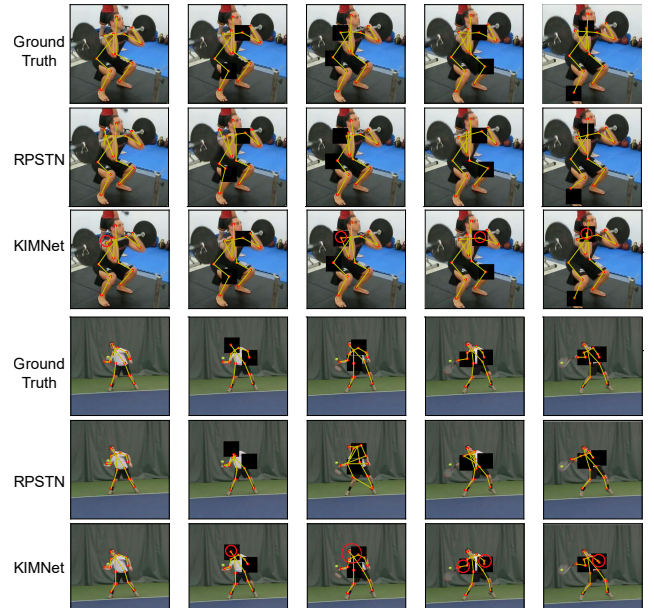


Fig. 8. Visualization of occluded poses. We use red circles to highlight the joints that are localized more accurate by KIMNet.

c) Influence of the number of occluded joints: To evaluate the influence of the number of occluded joints, the number of occluded joints is increased from 1 to 9. There are 13 joints in the pose of the Penn Action dataset. Therefore, occlusion of 9 joints can be regarded as severe occlusion. Under the same experimental settings, we compare the performance of the proposed KIMNet with existing methods, as shown in Fig.9. With the increase in the number of occluded joints, the performance of all models declines. However, compared to previous approaches, our KIMNet is more robust to the occlusion. It can be seen from Fig.9 that the performance of RPSTN declines sharply with the increase of occluded joints. When nine joints are occluded, the performance of KIMNet is about 85%, while the mPCK of RPSTN is less than 75%. The possible reason is that KIMNet explicitly models the temporal correlation between any two joints. In this way, it can use historically visible joints to help locate occluded joints in subsequent frames.

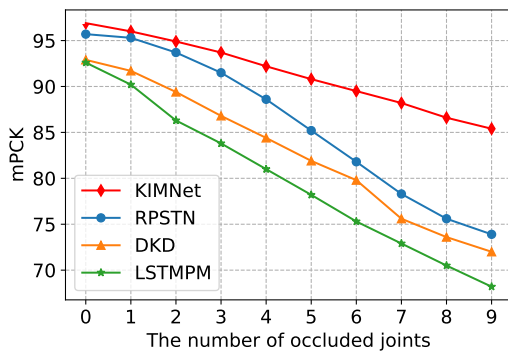


Fig. 9. Comparison of the performance between KIMNet and existing methods under the occlusion scene.

F. Comparisons of Performance without the Manual Occlusion

We also qualitatively compare the KIMNet with RPSTN [15] in the scene without adding manual masks. Qualitative results are depicted in Fig. 10. We have visualized poses of the ground truth (row 1 and row 4), outputs of RPSTN (row 2 and row 5), and outputs of our KIMNet (row 3 and row 6). We can see that our approach outputs more precise poses than the RPSTN. For example, for the action “weight lifting”, RPSTN locates the hip in the 1st frame, right ankles in the 3rd and 4th frames to the background. These joints are obviously located incorrectly. However, our KIMNet provides accurate positions for these joints (in green circles). Moreover, our KIMNet can give more reasonable positions for joints compared with the ground truth. For example, the hips provided by ground truth are far away from the body area. While the proposed KIMNet locates hips precisely. Besides, for the action “rope skipping”, the KIMNet also performs better than RPSTN. For example, the KIMNet can provide more accurate positions of right ankles than RPSTN in the 2nd, 3rd, and 4th frames. These benefits come from two aspects: 1) the proposed KMM explicitly models the temporal correlation between any two joints across different frames, which can guide the model to pay much attention to the body area. 2) KMM maintains the high resolution of feature maps. Thus, KMM is able to provide richer historical information on poses than the JRPSP used in RPSTN. Experimental results show that KIMNet shows superior performance in both occluded and non occluded scenes.

V. CONCLUSION

We propose a kinematic modeling network (KIMNet) for estimating human poses from videos. This work’s main contribution lies in designing a plug-and-play kinematics modeling module (KMM). The KMM is implemented based on the domain-cross attention mechanism, which allows it to maintain the high resolution of feature maps in historical frames. Hence, it can provide rich historical information about poses to help estimate poses from the current frame. Furthermore, the KMM explicitly models the temporal correlation between any two joints across different frames. In this way, KMM can learn the motion cues of each joint relative to all joints in the previous

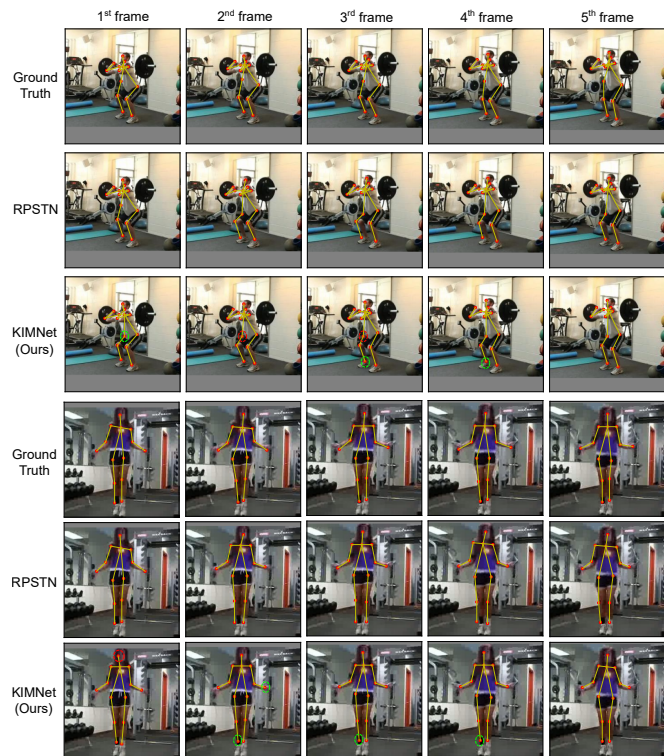


Fig. 10. Qualitative comparisons with existing method in the non occlusion scene. The 1st and 4th rows are the ground truth. The 2nd and 5th rows are the output of RPSTN. The 3rd and 6th rows are the output of the proposed KIMNet. Joints in green circles represent the joints that KIMNet locates more accurately than RPSTN. Joints in red circles represent the joints that KIMNet locates worse than RPSTN.

frame. And it can infer the positions of occluded joints at present according to all joints at the last moment. Experimental results show the advantages of our KIMNet in achieving state-of-the-art results on two challenging benchmarks. However, there is a drawback to the proposed KIMNet. The performance of KIMNet is limited by the long-term temporal modeling capability. Therefore, we will concentrate on improving the long-term temporal modeling ability of the KIMNet.

ACKNOWLEDGMENTS

This work was supported partly by the National Natural Science Foundation of China (Grant No. 62173045, 61673192), partly by the Fundamental Research Funds for the Central Universities (Grant No. 2020XD-A04-3), and the Natural Science Foundation of Hainan Province (Grant No. 622RC675).

REFERENCES

- [1] Z. Liu, R. Feng, H. Chen, S. Wu, Y. Gao, Y. Gao, and X. Wang, “Temporal feature alignment and mutual information maximization for video-based human pose estimation,” *CoRR*, vol. abs/2203.15227, 2022.
- [2] U. Iqbal, M. Garbade, and J. Gall, “Pose for action - action for pose,” in *Proc. IEEE International Conf. Automatic Face & Gesture Recognition (FG)*, Washington, DC, USA, 2017, pp. 438–445.
- [3] W. Du, Y. Wang, and Y. Qiao, “RPAN: an end-to-end recurrent pose-attention network for action recognition in videos,” in *Proc. IEEE International Conf. Computer Vision (ICCV)*, Venice, Italy, 2017, pp. 3745–3754.

- [4] D. Pham, "Human identification using neural network-based classification of periodic behaviors in virtual reality," in *Proc. IEEE Conf. Virtual Reality and 3D User Interfaces (VR), Tuebingen/Reutlingen, Germany*, K. Kiyokawa, F. Steinicke, B. H. Thomas, and G. Welch, Eds., 2018, pp. 657–658.
- [5] J. Banzi, I. Bulugu, and Z. Ye, "Learning a deep predictive coding network for a semi-supervised 3d-hand pose estimation," *IEEE CAA J. Autom. Sinica*, vol. 7, no. 5, pp. 1371–1379, 2020.
- [6] T. Zhang, J. Xiao, L. Li, C. Wang, and G. Xie, "Toward coordination control of multiple fish-like robots: Real-time vision-based pose estimation and tracking via deep neural networks," *IEEE CAA J. Autom. Sinica*, vol. 8, no. 12, pp. 1964–1976, 2021.
- [7] W. Liu, Q. Bao, Y. Sun, and T. Mei, "Recent advances in monocular 2d and 3d human pose estimation: A deep learning perspective," *CoRR*, vol. abs/2104.11536, 2021.
- [8] Y. Luo, J. S. J. Ren, Z. Wang, W. Sun, J. Pan, J. Liu, J. Pang, and L. Lin, "LSTM pose machines," in *Proc. IEEE Conf. Computer Vision and Pattern Recognition (CVPR), Salt Lake City, UT, USA*, 2018, pp. 5207–5215.
- [9] S. Zuffi, J. Romero, C. Schmid, and M. J. Black, "Estimating human pose with flowing puppets," in *Proc. IEEE International Conf. Computer Vision (ICCV), Sydney, Australia*, 2013, pp. 3312–3319.
- [10] T. Pfister, J. Charles, and A. Zisserman, "Flowing convnets for human pose estimation in videos," in *Proc. IEEE International Conference on Computer Vision (ICCV), Santiago, Chile*, 2015, pp. 1913–1921.
- [11] D. Zhang and M. Shah, "Human pose estimation in videos," in *Proc. IEEE International Conference on Computer Vision (ICCV), Santiago, Chile*, 2015, pp. 2012–2020.
- [12] R. Girdhar, G. Gkioxari, L. Torresani, M. Paluri, and D. Tran, "Detect-and-track: Efficient pose estimation in videos," in *Proc. IEEE Conf. Computer Vision and Pattern Recognition (CVPR), Salt Lake City, UT, USA*, 2018, pp. 350–359.
- [13] M. Wang, J. Tighe, and D. Modolo, "Combining detection and tracking for human pose estimation in videos," in *Proc. IEEE Conf. Computer Vision and Pattern Recognition (CVPR), Seattle, WA, USA*, 2020, pp. 11 085–11 093.
- [14] X. Nie, Y. Li, L. Luo, N. Zhang, and J. Feng, "Dynamic kernel distillation for efficient pose estimation in videos," in *Proc. IEEE International Conference on Computer Vision (ICCV), Seoul, Korea (South)*, 2019, pp. 6941–6949.
- [15] Y. Dang and J. Yin, "Relation-based associative joint location for human pose estimation in videos," *IEEE Trans. Image Process.*, vol. 31, pp. 3973–3986, 2022.
- [16] S. Wei, V. Ramakrishna, T. Kanade, and Y. Sheikh, "Convolutional pose machines," in *Proc. IEEE Conf. on Computer Vision and Pattern Recognition (CVPR), Las Vegas, NV, USA*, 2016, pp. 4724–4732.
- [17] W. Tang, P. Yu, and Y. Wu, "Deeply learned compositional models for human pose estimation," in *Proc. European Conf. Computer Vision (ECCV), Munich, Germany*, V. Ferrari, M. Hebert, C. Sminchisescu, and Y. Weiss, Eds., vol. 11207, 2018, pp. 197–214.
- [18] Q. Dang, J. Yin, B. Wang, and W. Zheng, "Deep learning based 2d human pose estimation: a survey," *Tsinghua Science and Technology*, vol. 24, no. 006, pp. 663–676, 2019.
- [19] Y. Chen, Z. Wang, Y. Peng, Z. Zhang, G. Yu, and J. Sun, "Cascaded pyramid network for multi-person pose estimation," in *Proc. IEEE Conf. on Computer Vision and Pattern Recognition (CVPR), Salt Lake City, UT, USA*, 2018, pp. 7103–7112.
- [20] K. Sun, B. Xiao, D. Liu, and J. Wang, "Deep high-resolution representation learning for human pose estimation," in *Proc. IEEE Conf. on Computer Vision and Pattern Recognition (CVPR), Long Beach, CA, USA*, 2019, pp. 5693–5703.
- [21] Y. Wu, D. Kong, S. Wang, J. Li, and B. Yin, "An unsupervised real-time framework of human pose tracking from range image sequences," *IEEE Trans. Multimed.*, vol. 22, no. 8, pp. 2177–2190, 2020.
- [22] A. Kamel, B. Sheng, P. Li, J. Kim, and D. D. Feng, "Hybrid refinement-correction heatmaps for human pose estimation," *IEEE Trans. Multimed.*, vol. 23, pp. 1330–1342, 2021.
- [23] D. Park and D. Ramanan, "N-best maximal decoders for part models," in *Proc. IEEE International Conf. on Computer Vision (ICCV), Barcelona, Spain*, D. N. Metaxas, L. Quan, A. Sanfeliu, and L. V. Gool, Eds., 2011, pp. 2627–2634.
- [24] B. X. Nie, C. Xiong, and S. Zhu, "Joint action recognition and pose estimation from video," in *Proc. IEEE Conf. on Computer Vision and Pattern Recognition (CVPR), Boston, MA, USA*, 2015, pp. 1293–1301.
- [25] J. Charles, T. Pfister, D. R. Magee, D. C. Hogg, and A. Zisserman, "Personalizing human video pose estimation," in *Proc. IEEE Conf. on Computer Vision and Pattern Recognition (CVPR), Las Vegas, NV, USA*, 2016, pp. 3063–3072.
- [26] J. Song, L. Wang, L. V. Gool, and O. Hilliges, "Thin-slicing network: A deep structured model for pose estimation in videos," in *Proc. IEEE Conf. on Computer Vision and Pattern Recognition (CVPR), Honolulu, HI, USA*, 2017, pp. 5563–5572.
- [27] J. Hwang, J. Lee, S. Park, and N. Kwak, "Pose estimator and tracker using temporal flow maps for limbs," in *Proc. International Joint Conf. on Neural Networks (IJCNN), Budapest, Hungary*, 2019, pp. 1–8.
- [28] H. S. and S. J., "Long short-term memory," *Neural Computation*, vol. 9, no. 8, pp. 1735–1780, 1997.
- [29] M. Li, Z. Zhou, and X. Liu, "Multi-person pose estimation using bounding box constraint and LSTM," *IEEE Trans. Multimed.*, vol. 21, no. 10, pp. 2653–2663, 2019.
- [30] M. Okada, S. Takenaka, and T. Taniguchi, "Multi-person pose tracking using sequential monte carlo with probabilistic neural pose predictor," in *Proc. IEEE International Conf. on Robotics and Automation (ICRA), Paris, France*, 2020, pp. 10 024–10 030.
- [31] B. Artacho and A. E. Savakis, "Unipose: Unified human pose estimation in single images and videos," in *Proc. IEEE Conf. on Computer Vision and Pattern Recognition (CVPR), Seattle, WA, USA*, 2020, pp. 7033–7042.
- [32] B. Xiao, H. Wu, and Y. Wei, "Simple baselines for human pose estimation and tracking," in *Proc. European Conf. Computer Vision (ECCV), Munich, Germany*, V. Ferrari, M. Hebert, C. Sminchisescu, and Y. Weiss, Eds., vol. 11210, 2018, pp. 472–487.
- [33] R. Girdhar, G. Gkioxari, L. Torresani, M. Paluri, and D. Tran, "Detect-and-track: Efficient pose estimation in videos," in *Proc. IEEE Conf. on Computer Vision and Pattern Recognition (CVPR), Salt Lake City, UT, USA*, 2018, pp. 350–359.
- [34] M. Wang, J. Tighe, and D. Modolo, "Combining detection and tracking for human pose estimation in videos," in *Proc. IEEE Conf. on Computer Vision and Pattern Recognition (CVPR), Seattle, WA, USA*, 2020, pp. 11 085–11 093.
- [35] S. Jin, W. Liu, W. Ouyang, and C. Qian, "Multi-person articulated tracking with spatial and temporal embeddings," in *Proc. IEEE Conf. on Computer Vision and Pattern Recognition (CVPR), Long Beach, CA, USA*, 2019, pp. 5664–5673.
- [36] Y. Zhang, Y. Wang, O. I. Camps, and M. Szaier, "Key frame proposal network for efficient pose estimation in videos," in *Proc. European Conference Computer Vision (ECCV), Glasgow, UK*, A. Vedaldi, H. Bischof, T. Brox, and J. Frahm, Eds., vol. 12362, 2020, pp. 609–625.
- [37] A. Bulat and G. Tzimiropoulos, "Human pose estimation via convolutional part heatmap regression," in *Proc. European Conference Computer Vision (ECCV), Amsterdam, The Netherlands*, B. Leibe, J. Matas, N. Sebe, and M. Welling, Eds., 2016, pp. 717–732.
- [38] L. Fu, J. Zhang, and K. Huang, "ORGM: occlusion relational graphical model for human pose estimation," *IEEE Trans. Image Process.*, vol. 26, no. 2, pp. 927–941, 2017.
- [39] G. Ning, Z. Zhang, and Z. He, "Knowledge-guided deep fractal neural networks for human pose estimation," *IEEE Trans. Multimed.*, vol. 20, no. 5, pp. 1246–1259, 2018.

- [40] J. Wang, X. Long, Y. Gao, E. Ding, and S. Wen, "Graph-pcnn: Two stage human pose estimation with graph pose refinement," in *Proc. European Conf. Computer Vision (ECCV), Glasgow, UK*, A. Vedaldi, H. Bischof, T. Brox, and J. Frahm, Eds., 2020, pp. 492–508.
- [41] Y. Bin, Z. Chen, X. Wei, X. Chen, C. Gao, and N. Sang, "Structure-aware human pose estimation with graph convolutional networks," *Pattern Recognit.*, vol. 106, p. 107410, 2020.
- [42] X. Wang, R. B. Girshick, A. Gupta, and K. He, "Non-local neural networks," in *Proc. IEEE Conf. on Computer Vision and Pattern Recognition (CVPR), Salt Lake City, UT, USA*, 2018, pp. 7794–7803.
- [43] H. Xu, J. Zhang, J. Cai, H. Rezatofghi, and D. Tao, "Gmflow: Learning optical flow via global matching," in *Proc. of the IEEE Conf. on Computer Vision and Pattern Recognition (CVPR)*, June 2022, pp. 8121–8130.
- [44] W. Zhang, M. Zhu, and K. G. Derpanis, "From actemes to action: A strongly-supervised representation for detailed action understanding," in *Proc. IEEE International Conf. on Computer Vision (ICCV), Sydney, Australia*, 2013, pp. 2248–2255.
- [45] H. Jhuang, J. Gall, S. Zuffi, C. Schmid, and M. J. Black, "Towards understanding action recognition," in *Proc. IEEE International Conf. on Computer Vision (ICCV), Sydney, Australia*, 2013, pp. 3192–3199.
- [46] M. Andriluka, L. Pishchulin, P. V. Gehler, and B. Schiele, "2d human pose estimation: New benchmark and state of the art analysis," in *Proc. IEEE Conf. on Computer Vision and Pattern Recognition (CVPR), Columbus, OH, USA*, 2014, pp. 3686–3693.
- [47] D. P. Kingma and J. Ba, "Adam: A method for stochastic optimization," in *Proc. International Conf. on Learning Representations (ICLR), San Diego, CA, USA*, Y. Bengio and Y. LeCun, Eds., 2015.
- [48] G. Gkioxari, A. Toshev, and N. Jaitly, "Chained predictions using convolutional neural networks," in *Proc. European Conf. Computer Vision (ECCV), Amsterdam, The Netherlands*, 2016, pp. 728–743.
- [49] Y. Li, K. Li, X. Wang, and R. Y. D. Xu, "Exploring temporal consistency for human pose estimation in videos," *Pattern Recognit.*, vol. 103, p. 107258, 2020.
- [50] A. Newell, K. Yang, and J. Deng, "Stacked hourglass networks for human pose estimation," in *Proc. European Conf. Computer Vision (ECCV), Amsterdam, The Netherlands*, B. Leibe, J. Matas, N. Sebe, and M. Welling, Eds., 2016, pp. 483–499.



Yonghao Dang Yonghao Dang received his Bachelor degree in computer science and technology from the University of Jinan, Jinan, China, in 2018. He is currently a Ph.D. candidate with the School of Artificial Intelligence, Beijing University of Posts and Telecommunications, Beijing, China. His research interests include computer vision, machine learning and image processing, deep learning. Email: dyh2018@bupt.edu.cn.



Jianqin Yin Jianqin Yin received the Ph.D. degree from Shandong University, Jinan, China, in 2013. She currently is a Professor with the School of Artificial Intelligence, Beijing University of Posts and Telecommunications, Beijing, China. Her research interests include service robot, pattern recognition, machine learning and image processing. Email: jqyin@bupt.edu.cn.



Shaojie Zhang Shaojie Zhang is currently a Bachelors candidate with the School of Artificial Intelligence, Beijing University of Posts and Telecommunications, Beijing, China. His research interests include computer vision, deep learning. Email: zsj@bupt.edu.cn.



Jiping Liu Jiping Liu received the Ph.D. degree from the PLA Information Engineering University. Mapping, in 2004. He currently is a Professor with the Chinese Academy of Surveying and Mapping. His research interests include the analysis of geographical conditions, emergency geographic information service, geospatial big data analysis, E-government geographic information service, on-line geographic information monitoring and spatial decision-making.



Yanzhu Hu Yanzhu Hu was born in Beijing, China, in 1970. He received the B.S. degree in control science and engineering from the Beijing University of Aeronautics and Astronautics, in 1991, the M.S. degree in economic management from the Chinese Academy of Social Sciences, in 1997, and the Ph.D. degree in systems engineering from Beijing Jiaotong University, in 2005. From 2006 to 2007, he did his Postdoctoral Research at Beijing Jiaotong University. Since 2008, he has been a Professor with the School of Automation, Beijing University of Posts and Telecommunications. He is the author of more than 15 articles. His research interests include intelligent monitoring and image processing.